JOURNAL OF PROPULSION AND POWER
Vol. 24, No. 1, January–February 2008

Concentration Distribution in a Supersonic Flow Recirculation Region

Amit Thakur* and Corin Segal†
University of Florida, Gainesville, Florida 32611

DOI: 10.2514/1.25396

Flameholding in supersonic flow depends on the local conditions in the recirculation region and the mass transfer into and out of this region. Large gradients in local gas composition and temperature exist in the recirculation region; hence, stability parameter correlations developed for premixed flames cannot be used to determine the blowout stability limits for nonpremixed flames encountered in practical devices. In the present investigation, mixture samples were extracted at different locations in the recirculation region and shear layer formed behind a rearward-facing step and were analyzed by a mass spectrometer to determine the distribution of species concentration in the region. Both nonreacting flow tests and combustion experiments were performed for a range of fuel-related parameters such as injection location, injection pressure, and fuel type. The difference between the local fuel mole fraction within the recirculation region determined from mass spectrometry and the global fuel mole fraction based on the total moles of air and fuel injected was identified. Planar-laser-induced fluorescence was used in nonreacting cases to provide a two-dimensional image of fuel distribution and complement the mass spectrometry measurements. Differences between local concentrations and estimates based on overall global injected mass flows were large, amounting to an order of magnitude. This implies significant differences in flame stability limits of a nonpremixed flame in supersonic flow compared to premixed flame.

Nomenclature

Da	=	Damköhler number
H	=	step height, 12.5 mm
M	=	Mach number
m/z	=	mass-to-charge ratio
P_0	=	stagnation pressure, atm
q_r	=	$\rho_{\text{fuel}} V_{\text{fuel}}^2 / \rho_{\text{air}} V_{\text{air}}^2$
T_0	=	stagnation temperature, K
V	=	velocity, m/s
W	=	duct half-width at the test-section entrance, 12.5 mm
X	=	mole fraction
ρ	=	density, kg/m^3
φ	=	equivalence ratio

I. Introduction

FLAMEHOLDING is ensured when the fluid residence time available is larger than the fuel reaction time (i.e., a suitably selected Damköhler number: $Da = \tau_{\text{residence}}/\tau_{\text{reaction}} > 1$). Residence times are short in a supersonic combustion chamber, on the order of only a few milliseconds, thus comparable with hydrogen chemical reaction times and significantly higher for hydrocarbon-based fuels. A recirculation region that extends the residence time is therefore used. This flameholding region serves as a reservoir of radicals that sustain the flame and propagate combustion in the main supersonic flow.

Even in a simple geometry used to generate a flameholding region in supersonic flow, such as a rearward-facing step, the flow structure is quite complex and three-dimensional. The approaching airflow boundary layer separates at the step and forms a shear layer between the supersonic flow and the subsonic recirculation region. Depending on the amount of heat released in this region, an expansion or a compression will dictate the length and shape of the recirculation region. If fuel is injected directly into the recirculation region, then additional shear layers appear around the jet boundaries, in which the flame is initiated followed by mixing and heat exchange between the hot gases in the region. Thus, a primary recirculation of gases exists that engulfs the recirculation region with additional smaller recirculations present. Even in a two-dimensional geometry, the presence of walls leads to a complex 3-D flow pattern. In this complex flow, large local equivalence ratio can exist even when the global equivalence ratio indicates an overall lean mixture [1]. Fresh-air penetration into the recirculation region and the supply of hot combustion radicals out into the main flow occur through the detached shear layer. The shear-layer growth and mass exchange depend on a host of parameters including velocity ratio, density ratio, convective Mach numbers, heat release, and local pressure gradient [2].

A substantial database of flame stability exists for premixed gases [3–5], from which stability limits for rich and lean flames were obtained for a number of fuel mixtures. The stability limit has usually been cast in terms of the flameholding boundary on an equivalence ratio vs a carefully selected stability-parameter plane. These stability parameters depend on the flow velocity, temperature, size, and shape of the flameholder and have received various formulations in different studies, from empirical formulations to expressions that reflect global Damköhler numbers [6–8].

In the case of nonpremixed gases, the determination of stability limits is less straightforward, primarily due to the nonhomogeneity of the parameters in the flameholder's recirculation region resulting from the presence of large concentration and temperature gradients and the complex 3-D flow structure. These difficulties are compounded by the uncertainty in the shape of the recirculation region, which is a function of the amount of heat release, which in turn is dictated by the local mixing and combustion efficiencies.

Ortwerth et al. [1] modified Ozawa's [3] stability parameter for premixed gases by including locally measured parameters in the recirculation region with limited success. The new parameter managed to describe a stability boundary for low equivalence ratios for hydrogen combustion but failed at injected equivalence ratios in excess of 0.1. Driscoll and Rasmussen [9] performed an analysis intended to lead to the development of a correlation for nonpremixed flame stability limits in supersonic flow based on the suggestion that

Received 23 May 2006; revision received 6 August 2007; accepted for publication 7 August 2007.

*Graduate Research Assistant, Mechanical and Aerospace Engineering.
†Associate Professor, Mechanical and Aerospace Engineering. Associate Fellow AIAA.

the flame is sustained in the shear layer and not in the bulk of recirculation region. Flame propagation speed along the stoichiometric contour in the shear layer is matched in this analysis by the velocity of the incoming gas. Hot products in the recirculation zone preheat the shear-layer gases and increase the flame propagation speed. Flame blowout is then governed by the imbalance between flame propagation speed and gas velocity. Some additional parameters governing blowout appeared in the nonpremixed flame correlation compared with the premixed flame correlation: fuel-injection location relative to the recirculation region, fuel-injection temperature, and stoichiometric fuel mixture fraction. A limitation of this correlation is that a global fuel equivalence ratio is used to obtain the flame stability curve, which is quite different from the local equivalence ratio in the flameholding recirculation region.

Rasmussen et al. [10] examined the stability of hydrocarbon flames in supersonic flow using cavity flameholders. Fuel was injected from the cavity floor or from the forward cavity wall. The lean and rich flame blowout limits showed strong dependence on the fuel-injection location within the cavity. Winterfeld [11] performed flame blowout experiments in supersonic flow, using a contoured cylindrical flameholder and a cone-cylinder flameholder for which which hydrogen was injected upstream of the recirculation region formed in the flameholder's base or directly into it. The flame blowout curve was sensitive to the fuel-injection angle, evidencing the importance of the fuel-injection location relative to the flameholding recirculation region. The recirculation region length was used along with the nozzle exit velocity to infer a characteristic residence time and, further, a Damköhler-number-based stability parameter. The results were limited by the absence of walls that, in a realistic environment, change the shape of the recirculation region, the local pressure, and hence the local equivalence ratios.

Several parameters affect nonpremixed flame stabilization in supersonic flow. Their effect would be better understood by knowledge of species-composition distribution in the flameholding recirculation region; however, few such measurements have been made so far for nonreacting flow experiments and fewer yet for reacting cases. Hsu et al. [12] used Raman scattering to measure fuel distribution inside a cavity in nonreacting supersonic flow using ethylene injected at a low angle upstream of the cavity. The effect of fuel-injection pressure, cavity size, and imposed backpressure on fuel transport in the cavity was studied. Following Hsu's experiments, Gruber et al. [13] made planar laser-induced fluorescence (PLIF) measurements in the cavity to examine the effect of fuel-injection location on the cavity flameholder performance in supersonic flow for nonreacting flow and combustion experiments. Uchiumi et al. [14] followed the Niioka et al. [15] investigation of flameholding using a strut divided into two parts.

Nonreacting flow measurements of the local equivalence ratio along the distance between the strut parts were used to improve its flameholding performance. Zamma et al. [16] measured pressure and gas composition for nonreacting supersonic flow over a step with fuel injected downstream of the step transverse to the airflow. The fuel volume fraction in the recirculation region was found to decrease with increasing fuel–air dynamic pressure ratio. Higher fuel volume fraction was observed in the recirculation region for lighter fuel compared with heavier fuel injected at the same dynamic pressure ratio.

Thayer and Corlett [17] measured pressure, temperature, and gas composition in the separated recirculation region upstream of a jet injected transverse to nonreacting supersonic airflow and found that a large part of the recirculation region had a nearly uniform fuel distribution; however, the region was fuel-rich in composition and it was estimated that approximately 5% of the injected fuel was entrained in the recirculation region. McDaniel et al. [18] made 3-D measurements of flow variables for a flowfield with staged transverse fuel injection downstream of a step in nonreacting supersonic flow. Large fuel concentration, close to stoichiometry, was observed in the recirculation region.

The latter two studies evidenced the sensitivity of the recirculation region concentration to the fuel-injection location. Strokin and Grachev [7] obtained experimental data on ignition and flameholding in supersonic flow using a cavity flameholder for a variety of experimental conditions from which a flame stability curve was derived. The equivalence ratio in the recirculation region was empirically estimated using air and fuel stagnation temperature, recirculation region static temperature, approaching airflow boundary-layer thickness, injection geometry, and overall air–fuel equivalence ratio. Morrison et al. [19] estimated the local equivalence ratio and mixing efficiency in the recirculation region behind a step by assuming complete mixed conditions in the region and a certain fixed percentage of air replenishment into the region.

Numerical simulations of fuel mole fraction in the recirculation region for various geometries have also contributed to flameholding studies. Kim et al. [20] evaluated flow oscillations as a measure of stability over a cavity with fuel injected either upstream or downstream of the cavity. The former produced significantly lower oscillations because it led to a more stable shear layer over the cavity. For downstream injection, fuel mole fraction contours showed that large vortices were present, entraining the fuel upstream into the cavity. Glawe et al. [21] simulated helium injection at the base of a strut in supersonic flow. The data showed a high helium mole fraction distribution in the recirculation region formed at the base of the strut.

There are limited experimental data regarding recirculation region composition for nonreacting flows and even scarcer information for reacting flows. The present study measured the nonpremixed concentration in the recirculation region formed behind a rearward step in supersonic flow in both nonreacting and reacting flows. A two-dimensional step was selected as the flameholder geometry because it is the simplest and a widely used configuration in supersonic combustor studies. Airflow parameters such as Mach number, stagnation pressure, and stagnation temperature were held constant. The fuel-related parameters such as injection location relative to the recirculation region, injection pressure, and fuel type were varied. Local species mole fraction and fuel equivalence ratio distribution in the recirculation region were measured with two methods for the nonreacting case: mass spectroscopy (MS) sampling (for both reacting and nonreacting cases) and acetone-based PLIF.

II. Experimental Setup

A. Supersonic Wind Tunnel

The supersonic wind tunnel used in the experiments provides direct connect tests with a variable combustion chamber entrance Mach number of 1.6–3.6 and stagnation temperatures corresponding to Mach 4.8 flight enthalpy. The wind tunnel is a continuously operating facility using a vitiated heater based on hydrogen combustion with oxygen replenishment to maintain a constant 0.21 oxygen mole fraction at all conditions, electronically controlled by a fuzzy logic controller [22]. All the experiments discussed here were performed with a combustion chamber entrance of Mach 1.6 and cold air (i.e., $T_{0\text{air}} = 300$ K). The Mach number corresponds to flight transition from ramjet to scramjet. A constant area isolator is placed between the nozzle and the combustor section with optical access to both the isolator and the test section from three sides. The isolator has a 25×25 mm^2 cross section and 170 mm length upstream of a rectangular rearward-facing step of height $H = 13$ mm and follows with a 51×25 mm^2 constant cross-sectional area test section of 330 mm ($26H$) in length. The test section is symmetric in geometry and fuel injection about the central plane. The airflow boundary-layer thickness at the isolator exit was 3.5 mm, or 13% of the duct height [23].

Fuel was injected, as shown in Fig. 1a, at sonic conditions at two locations:

1) At $0.3H$ downstream of the step, fuel was injected directly into the recirculation region from five 0.5-mm-diam holes equally spaced on each side, directed at 45 deg toward the step.

2) At $4H$ upstream of the step, fuel was injected from two 1.0-mm-diam holes equally spaced on each side of the isolator transverse to the airflow.

Helium (having a molecular weight close to hydrogen) and argon (having a molecular weight close to propane) were injected as

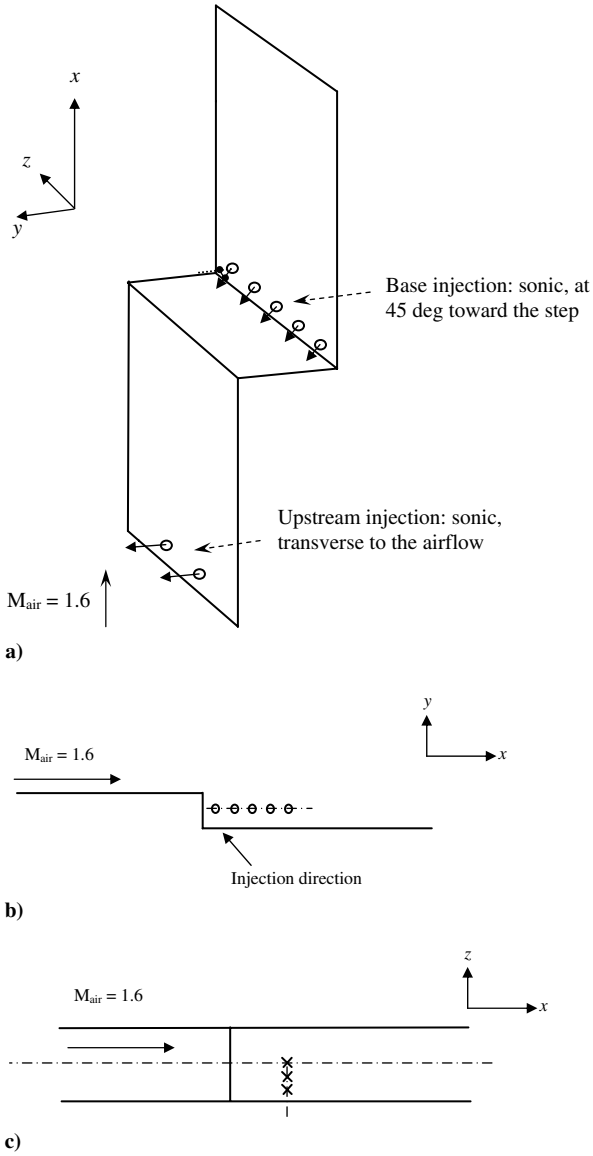

Fig. 1 Schematic diagrams of fuel injection and MS sampling locations in the test section: a) test-section and injection configuration, b) wall sampling ports, c) inflow sampling locations.

simulated fuel in nonreacting flow tests. Hydrogen was injected in combustion tests. MS was used to determine the sample species mole fraction distribution in the recirculation region. Acetone was seeded in the injectant and PLIF was used in nonreacting cases to infer a planar concentration of the injectant, as described next.

B. Mass Sampling and Analysis

The physical location of mass sampling ports in the recirculation region behind the step is shown in Figs. 1b and 1c. The coordinate system is also shown in the figures. Five mass sampling ports were placed along the wall in an axial x direction, equally spaced from $x/H = 0.5$ to 3.5 and along $y/H = 0.3$. These ports are 0.6-mm-inner-diam steel tubes that end at the test-section wall and do not physically intrude into the recirculation region (i.e., $z = 0$). In separate tests, other tubes are inserted into the flow, as shown in Fig. 1c, to measure the species special distribution inside the recirculation region. For nonreacting flow tests, three stainless steel tubes are placed at $x/H = 2.0$ and $y/H = 0.3$. This is the same x– y coordinate as port 3 in wall sampling (see Fig. 1b). These sampling tubes penetrate into the test section at three different depths, equally spaced in the inflow z direction from $z/W = 0.33$ to 1.0, where $W = 12.7$ mm is the test-section half-width. For combustion tests,

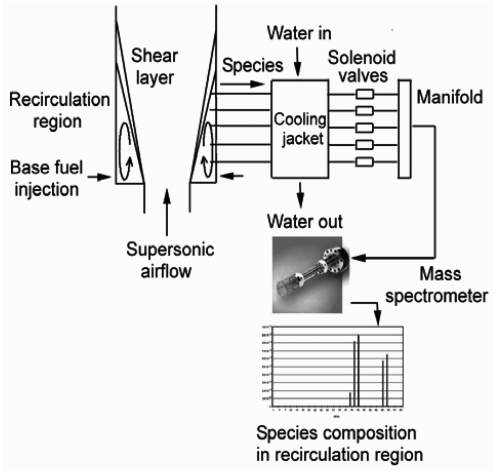

Fig. 2 Mass sampling and analysis diagram.

five 0.8-mm-inner-diam ceramic tubes are inserted to $z/W = 0.5$ from the wall at the same axial locations as the wall sampling ports.

A schematic diagram of mass sampling from the recirculation region and subsequent real-time analysis by a mass spectrometer is shown in Fig. 2. In combustion tests, the extracted species passed through a water-cooled jacket on their way to the mass spectrometer to quench the reactions and freeze the species composition coming out of the combustion chamber. The jacket was supplied with cold water at 283 K. The temperature drop experienced by the sampled mixture while passing through the cooling jacket resulted in condensation of water vapor and much of it did not reach the mass spectrometer. Hence, the corrected X_{H_2O}, shown in the subsequent figures, was deduced from the oxygen deficit in the product mixture.

The sampling tubes were then connected to a manifold having six 0.6-mm-diam input tubes and a single 1.8-mm-diam outlet tube connected to the mass spectrometer. The input of species to the manifold was regulated by a series of computer-controlled miniature solenoid valves that supply gas mixture from one sampling port at a time for analysis. Sampling from each port was preceded by a manifold purge with nitrogen to flush the species from the previous port, hence preventing the mixing of samples from two adjacent ports. The sampling time at each port and the purge time before each sampling were computer-controlled by the software.

The species were analyzed by a Stanford Research Systems RGA-300 mass spectrometer that uses electron ionization to ionize the sampled gas, an RF quadrupole filter to sort species according to their mass-to-charge ratio, and a Faraday cup to detect ion currents. The ionizer, filter, and detector are enclosed in a clean vacuum chamber and operate at pressure below 10^{-4} torr. The spectrometer can detect species up to a mass-to-charge ratio of 300 and has a resolution of 0.5 AMU at 10% peak height. The sensitivity factor of the instrument, defined as the signal detected per unit partial pressure of a given species (A/torr), varies for different gases. Hence, calibration of the instrument was performed for the helium, nitrogen, oxygen, and argon. The sensitivity factor of nitrogen was used as the baseline and sensitivity factors of the other gases were normalized with this baseline.

The species scanned were nitrogen ($m/z = 28$ and 14), oxygen ($m/z = 32$ and 16), helium ($m/z = 4$), and argon ($m/z = 40$ and 20) for nonreacting experiments and nitrogen, oxygen, hydrogen ($m/z = 2$ and 1), and water ($m/z = 18$ and 17) for combustion experiments. Sampling was done sequentially for 5 s at the purge port and for 20 s at each of the sampling ports. The spectrometer had a fast-response time of about 2–3 s to the change in gas composition while switching from one port to another. The local mole fraction of a given species in the sample was determined from the partial pressures of all the component species recorded by the mass spectrometer after time-averaging at each port over the sampling time period and correction using calibration factors for individual gases. The background level of argon in the incoming airflow for nonreacting experiments and the background levels of hydrogen and water for

combustion experiments were subtracted to determine the actual mole fractions of these species.

The sampled mole fractions are compared next with a global mole fraction determined from the total mole of fuel injected and the total mole of air traveling through the test section. Both local and global mole fractions/equivalence ratios are given in the results.

C. Acetone PLIF

PLIF was used by seeding acetone in the injectant and exciting it with a 266-nm, 0.5-mm-thick laser sheet in the x–y plane. The temperature distribution in the recirculation region is fairly uniform for nonreacting flows, and because the acetone LIF signal does not vary with temperature for the low-temperature range of 200–300 K [24], the signal-intensity variation in the corrected image was independent of temperature and varied only with acetone concentration. The acetone LIF signal at the fuel-injection location, for which fuel mole fraction is 100%, was taken as the reference point for other pixels in the image. The fuel mole fraction at a given pixel was then determined by the ratio of LIF intensity at that pixel to the LIF intensity at the reference point.

III. Results and Discussion

A. Nonreacting Flow

For the nonreacting cases, the air was maintained at $M_{\text{air}} = 1.6$, $T_{0\text{air}} = 300$ K, and $P_{0\text{air}} = 4.8$ atm. Helium and argon were injected as fuel simulants at two different pressures from the base of the step and from a location upstream of the step. Although the molecular weight of helium is close to hydrogen and argon has molecular weight close to propane, the data obtained from nonreacting flow tests cannot be directly extrapolated to combustion conditions absent the effects of heat release. The velocity and density gradients along the shear layer formed between the recirculation region and core airflow are different for nonreacting flow compared with reacting flow, and the mass exchange rate across the main airflow shear layer is higher for nonreacting flow compared with reacting flow [3]. For nonreacting flow, this would bring more air into the recirculation region; hence, the flameholding region may be leaner in fuel compared with reacting flow. However, the recirculation region for nonreacting flow is considerably smaller than that for reacting flow due to the absence of pressure rise caused by combustion balancing and, sometimes, overcoming the previous leaning condition. Despite these differences, nonreacting data indicate fuel distribution in the flameholding region just before ignition of the fuel–air mixture. Based on this information, the effect of various parameters such as fuel-injection pressure and location on flameholding characteristics in actual combustion can be estimated.

1. Base Injection

a. Helium. Helium was injected at two pressures: a moderate stagnation pressure $P_{0\text{He}} = 5.4$ atm and a high stagnation pressure $P_{0\text{He}} = 12.0$ atm, resulting in dynamic pressure ratios of 1.1 and 2.4, respectively. Correspondingly, the helium mass injection was 0.4 and 0.9 g/s. Each experiment was performed three times for repeatability; the average standard deviation in helium concentration X_{He} was 4%.

The wall pressure distribution for airflow without fuel injection is shown in Fig. 3, with the origin $x = 0$ corresponding to the step location. The airflow boundary-layer growth in the isolator effectively reduces the cross-sectional area and hence the pressure rise of supersonic flow approaching the step. The supersonic airflow expands at the step base, as indicated by the sharp drop in pressure at that location. The shear layer formed due to separation of the airflow boundary layer at the step base is pushed toward the wall and it reattaches downstream of the step. An oblique shock is formed at the reattachment point, causing a pressure rise at that location. Based on the wall pressure rise, the reattachment point is estimated to be between 1.5–2.0 H. The pressure distribution in the recirculation region remained unaffected by the fuel injection in the nonreacting

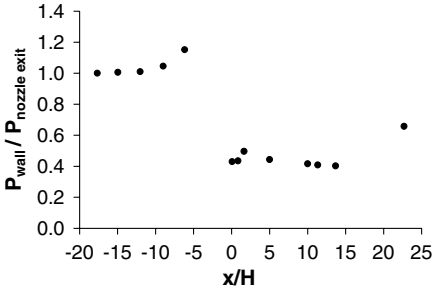

Fig. 3 Wall pressure distribution for nonreacting flow; $P_{0\text{air}} = 4.8$ atm and $M_{\text{air}} = 1.6$; the axial origin is placed at the step.

flow tests, indicating that fuel addition did not cause a substantial increase in the mass flow rate in the recirculation region.

The wall distribution of X_{He} in the recirculation region for the two $P_{0\text{He}}$ is shown in Fig. 4a. The standard deviation bars indicate experimental variation. The fuel-injection location is indicated on the horizontal axis. It is observed that the fuel mole fraction generally decreases in the x direction and away from the fuel-injection location, except the peak noticed for the higher q_r at the second port, which is a result of this particular injection configuration and would change for other design solutions.

The X_{He} distribution shows more nonuniformity at higher $P_{0\text{He}}$. Increasing $P_{0\text{He}}$ results in a corresponding increase in X_{He}, indicating that a considerable amount of the injected fuel remains in the recirculation region. This leads to rich local mixtures, as will be shown subsequently. Mass sampling in the inflow z direction for the same airflow and fuel-injection conditions is shown in Fig. 4b. The inflow sampling was done at $x/H = 2.0$ and $y/H = 0.3$. At both

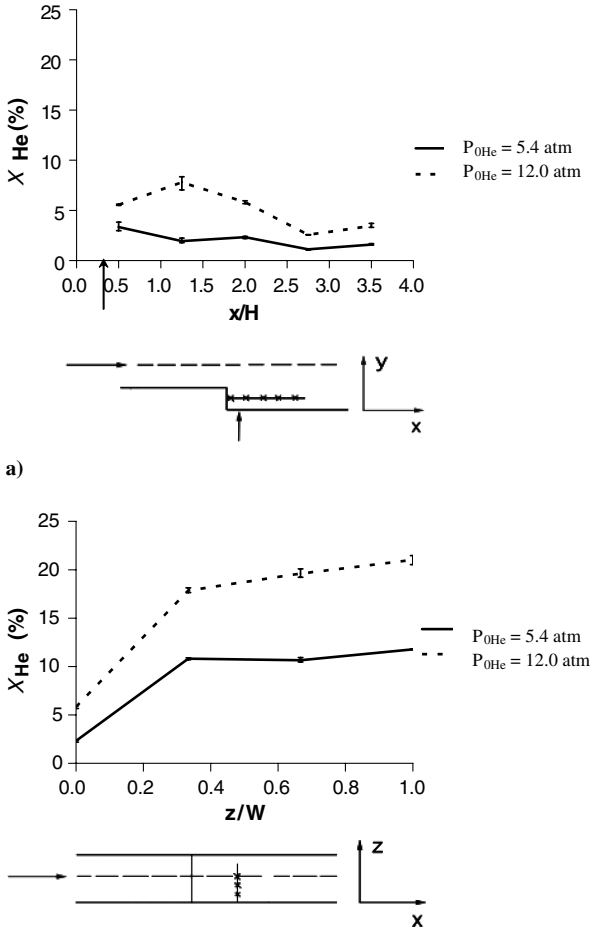

Fig. 4 Base fuel injection: helium mole fraction distribution in the recirculation region for a) wall sampling and b) inflow sampling; $P_{0\text{air}} = 4.8$ atm, $M_{\text{air}} = 1.6$, and $q_r = 1.1$ and 2.4.

Table 1 Helium base fuel injection: global and local X_{He}

P_{0He}, atm	Local X_{He}, %	Global X_{He}, %	Local/global X_{He}
	Wall sampling		
5.4	1.1–3.8	1.1	0.9–3.4
12.0	2.6–8.3	2.5	1.0–3.4
	Inflow sampling		
5.4	2.2–11.8	1.1	1.9–10.4
12.0	5.7–21.5	2.5	2.3–8.7

pressures, the inflow X_{He} are much higher than the wall measured X_{He} (specifically, up to four–five times). However, X_{He} distribution away from the wall is rather uniform, indicating a well-mixed fuel–air mixture at the axial location probed. The lower helium concentration in the wall vicinity may be due to the presence of additional recirculations near the wall that develop perpendicular to the main recirculation [1]. These generally large recirculations conceivably remove the injectant from the wall vicinity.

Table 1 indicates the locally and globally measured X_{He} for wall and inflow samplings. The global X_{He}, defined earlier, is obtained from the total moles of helium injected and the total moles of air flowing through the test section. For both cases, the locally measured X_{He} is up to three times more than the global estimate near the wall and about 10 times more for inflow sampling. This indicates that even when the overall engine mixture is lean, the recirculation region may be considerably richer, leading to flame blowout in the rich branch. This behavior was noticed in previous studies [25] based on local temperature measurements.

Helium has a molecular weight close to hydrogen; hence, the X_{He} distribution obtained from wall and inflow samplings is estimated to indicate that of hydrogen injected under identical test conditions. Using this assumption, if hydrogen had been injected, the local equivalence ratios of hydrogen, φ_{H_2}, could be determined from the local mole fraction measurements. For $P_{0H_2} = 5.4$ atm, the local φ_{H_2} could be as high as 0.4 for global $\varphi_{H_2} = 0.04$, whereas at the higher pressure, the local φ_{H_2} could be as high as 0.7 for global $\varphi_{H_2} = 0.1$. The high concentration of injectant indicates that a relatively small mass exchange takes place through the shear layer. References [17,19] suggest that the total mass exchange through the shear layer (and therefore the entire fuel–air mixture) amounts to 5% of the total mass flow. Hence, analyses based on global φ_{H_2} vastly underestimate the richness in the flameholding recirculation region.

PLIF of fuel distribution at the recirculation region center plane with helium injected at $P_{0He} = 5.4$ and 12.0 atm are shown in Figs. 5 and 6. The average standard deviation in helium concentration, X_{He}, due to the temporal variation in laser sheet profile was 8%. The PLIF image for $P_{0He} = 5.4$ atm is shown in Fig. 5a and the X_{He} distribution is shown in Fig. 5b. Figure 5a shows qualitatively that most of the injectant remains in a region close to the step with a considerably more uniform distribution in the rest of the recirculation region, similar to the findings of Thayer and Corlett [17]. Most of the fuel remains in the recirculation region even as the injection pressure was increased, as shown in Fig. 6. The X_{He} distribution shows that the distribution nonuniformity increases at higher injection pressure.

At the location at which PLIF and MS overlap, the results show a 8–10% mole fraction difference between the two methods. With the observation that $\varphi_{H_2} = 1$ corresponds to 30% X_{H_2} in a hydrogen–air mixture, it is seen in both Figs. 5 and 6 that a considerable part of the recirculation region is fuel-rich despite a low global φ_{H_2}. Figure 6 shows that for $P_{0He} = 12.0$ atm, the entire recirculation region, excluding a region near the shear layer, has $\varphi_{H_2} > 1$.

b. Argon. Argon was injected at the base of the step for the same airflow and fuel-injection pressure as in the case of helium. Thess conditions corresponded to argon mass injection of 3.2 and 7 g/s. The average standard deviation in X_{Ar} was 3%. The wall distribution of X_{Ar} in the recirculation region for the two P_{0Ar} is shown in Fig. 7a. The X_{Ar} distribution pattern is similar to that for helium injection, especially for low injection pressure, with the inflow X_{Ar} measurements up to two–three times higher than the wall-measured X_{Ar}, similar to the helium case.

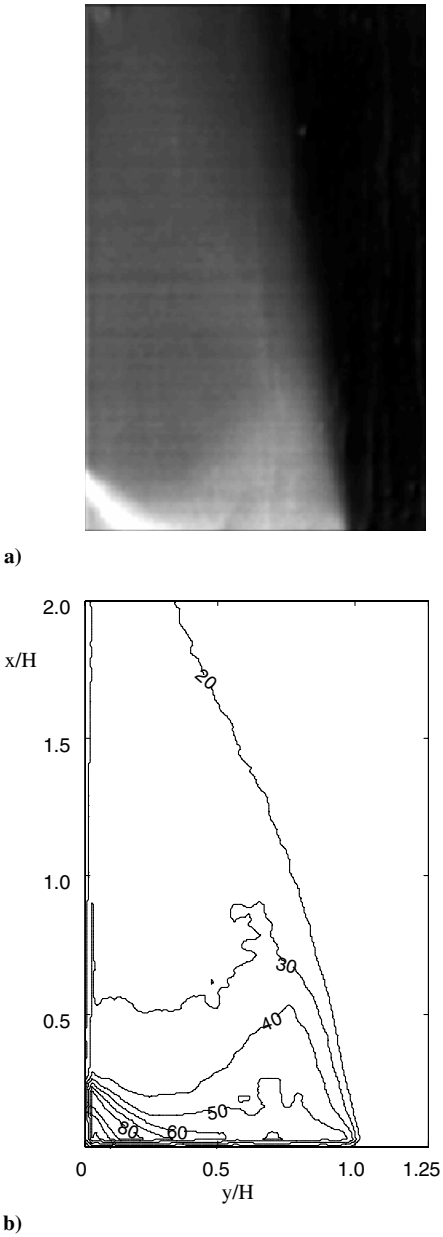

Fig. 5 PLIF measurement for helium base injection: a) fluorescence image and b) X_{He} distribution percentage; $q_r = 1.1$.

The locally and globally measured X_{Ar} for wall and inflow samplings are shown in Table 2, indicating inflow concentrations as high as 27 times for the low pressure and 21 times for the high pressure relative to the globally injected material. A comparison with the helium case shows that the local-to-global X_{fuel} ratio is higher for argon than for helium; that is, a higher concentration of argon is found in the recirculation region than for helium for a unit mole fraction of fuel injected in the test section. Because the residence time is long in the recirculation region, diffusion may be significant. The binary diffusion coefficient of a gas in air is inversely proportional to the square root of its molecular weight; hence, argon diffuses about three times slower in air compared with helium.

Argon has a molecular weight close to propane; hence, the X_{Ar} distribution obtained from the wall and inflow samplings is approximated to be same as that of propane injected under identical test conditions. For $P_{0C_3H_8} = 5.4$ atm, the local $\varphi_{C_3H_8}$ would be in the range of 0.5–2.5 for a global $\varphi_{C_3H_8} = 0.1$. For $P_{0C_3H_8} = 12.0$ atm, the local $\varphi_{C_3H_8}$ is estimated in the range of 1.0 – 4.3 for global $\varphi_{C_3H_8} = 0.2$. This shows that a fuel-rich mixture exists in the recirculation region even as the global $\varphi_{C_3H_8}$ suggests a fuel-lean

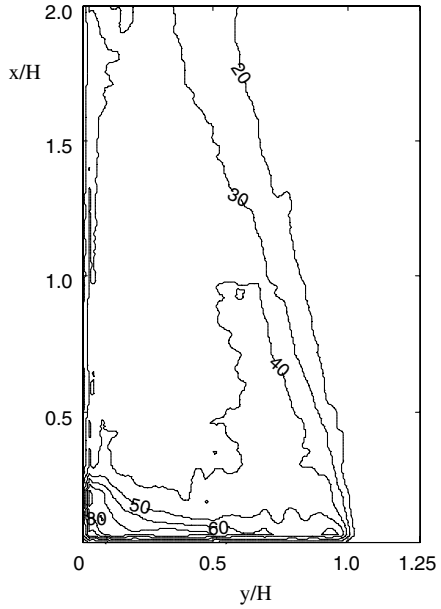

Fig. 6 PLIF measurement for base injection of helium X_{He} distribution percentage; $q_r = 1.1$.

mixture similar with helium findings in this study and previous investigations [18].

PLIF imaging of argon injection shown in Figs. 8 and 9 indicated considerable amounts remaining in the recirculation region close to the step base. If argon is thought of as a substitute for propane and the X_{Ar} distribution is similar to that of propane injected under identical test conditions, for $P_{0C_3H_8} = 5.4$ atm, the global $\varphi_{C_3H_8} = 0.1$ and for $P_{0C_3H_8} = 12.0$ atm, the global $\varphi_{C_3H_8} = 0.2$, both lean conditions. With the observation that $\varphi_{C_3H_8} = 1$ corresponds to 4% $X_{C_3H_8}$ in a propane–air mixture, it is seen in Figs. 8 and 9 that for both injection pressures, the entire recirculation region and the main airflow shear layer is fuel-rich in composition, with $\varphi_{C_3H_8} > 2$. A comparison with the MS results shows a difference of 6% in mole fraction in the low-pressure case and almost the same result for the higher injection pressure.

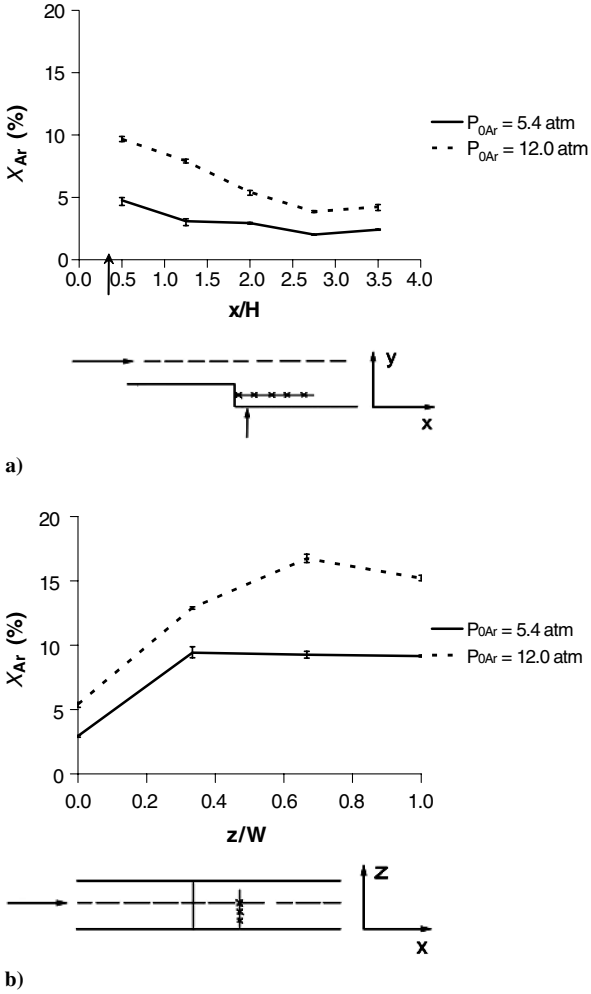

Fig. 7 Base fuel injection: Argon mole fraction distribution in the recirculation region for a) wall sampling and b) inflow sampling; $P_{0air} = 4.8$ atm and $M_{air} = 1.6$.

Table 2 Argon base fuel injection: global and local X_{Ar}

P_{0Ar}, atm	Local X_{Ar}, %	Global X_{Ar}, %	Local/global X_{Ar}
	Wall sampling		
5.4	2.0–5.0	0.4	5.5–13.9
12.0	3.8–9.9	0.8	4.9–12.7
	Inflow sampling		
5.4	2.9–9.9	0.4	7.9–27.4
12.0	5.2–17.1	0.8	6.6–21.9

2. Upstream Injection

a. Helium. Helium was injected upstream of the step through underexpanded jets transverse to the airflow, as shown in Fig. 1, at $P_{0He} = 2.4$ and 5.1 atm. The corresponding dynamic pressure ratios q_r were 0.5 and 1.0, respectively, and the injected mass flows were 0.7 and 1.5 g/s, respectively. The wall distribution of X_{He} in the recirculation region for the two cases is shown in Fig. 10a and the inflow distribution is shown in Fig. 10b. The inflow sampling shows an almost proportional increase in X_{He} with P_{0He}. The maximum helium concentration is at the port downstream of the injector, indicating that the concentration is no longer as uniform as seen for the base injection in Fig. 4. The plots show quite low levels of X_{He} in the recirculation region, hence indicating that upstream injection of helium can be effective to supply fuel to the recirculation region in amounts that would maintain equivalence ratios appropriate for flame piloting. Table 3 summarizes the local and global X_{He} for wall and inflow samplings. In fact, the local X_{He} is lesser than global X_{He}, indicating that the light gas penetrates through the main airflow boundary layer formed upstream of the step and only a small quantity

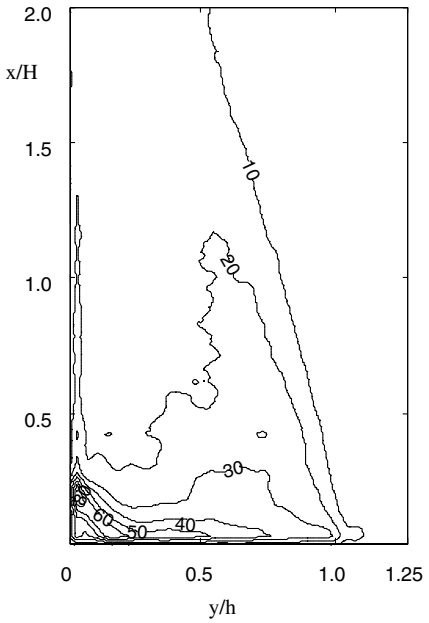

Fig. 8 PLIF measurement for argon base injection of argon X_{Ar} distribution percentage; $P_{0Ar} = 5.4$ atm, $P_{0air} = 4.8$ atm, and $M_{air} = 1.6$.

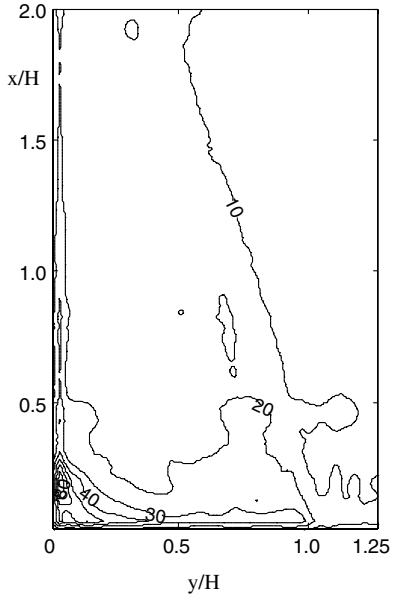

Fig. 9 PLIF measurement for argon base injection X_{Ar} distribution percentage; $P_{0Ar} = 12.0$ atm, $P_{0air} = 4.8$ atm, and $M_{air} = 1.6$.

is entrained into the recirculation region. The lean conditions in the recirculation region using this method could explain the increased flame stability with less flowfield oscillations than noted by Kim et al. [20] in their computation.

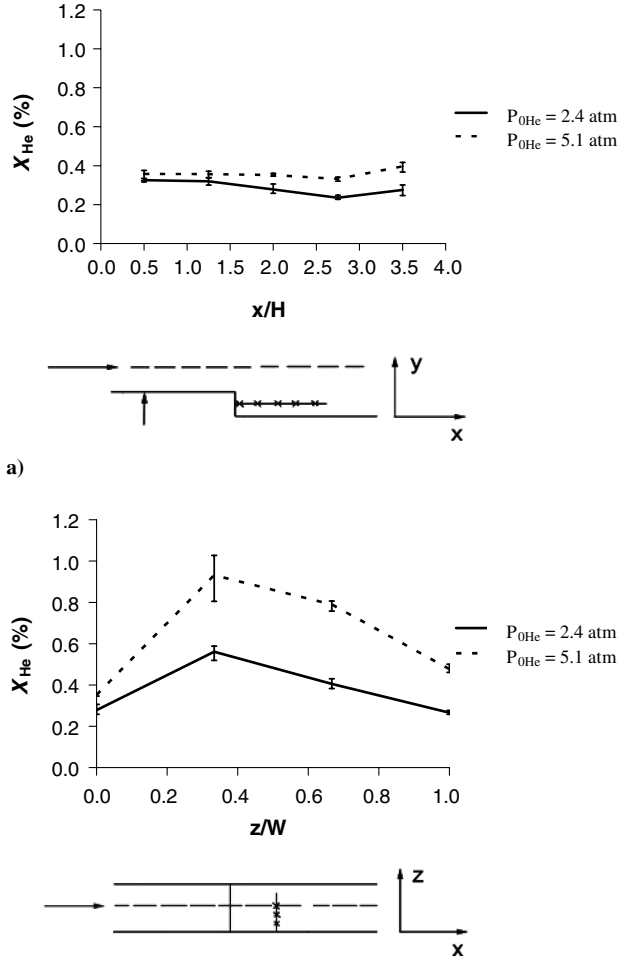

Fig. 10 Helium upstream injection; mole fraction distribution in the recirculation region for a) wall sampling and b) inflow sampling; $P_{0air} = 4.8$ atm and $M_{air} = 1.6$.

Table 3 Helium upstream fuel injection: global and local X_{He}

P_{0He}, atm	Local X_{He}, %	Global X_{He}, %	Local/global X_{He}
	Wall sampling		
2.4	0.2–0.3	0.7	0.3–0.5
5.1	0.3–0.4	1.5	0.2–0.3
	Inflow sampling		
2.4	0.3–0.6	0.7	0.4–0.9
5.1	0.4–1.0	1.5	0.2–0.7

With hydrogen, for $P_{0H_2} = 2.4$ atm, the local φ_{H_2} is estimated in the range of 0.01–0.02 for global $\varphi_{H_2} = 0.02$. For $P_{0H_2} = 5.1$ atm, the local φ_{H_2} is estimated in the range of 0.01–0.03 for global $\varphi_{H_2} = 0.05$. Hydrogen injected in the same amount would have a dynamic pressure ratio of 15% less than helium and so, proportionally, more would be expected in the recirculation region.

b. Argon. Argon injected upstream of the step for same airflow and same dynamic pressure ratio as in the case of helium resulted in wall and inflow distributions as shown in Fig. 11a and 11b, respectively. Injected argon mass flows were 0.9 and 2 g/s, respectively. Although the same general trend as for helium is obtained, the peak argon is found closer to the centerline. Table 4 summarizes the local and global X_{Ar} for wall and inflow samplings. Unlike the case of helium, the heavier gas argon reaches the recirculation region in quantities larger than the global X_{Ar}. It can be seen from the plots and from the local-to-global X_{Ar} ratios in the table that an increase in the upstream P_{0Ar} does not result in a corresponding increase in the amount of fuel reaching the recirculation region as much of the injectant penetrates beyond the boundary layer in the core supersonic flow.

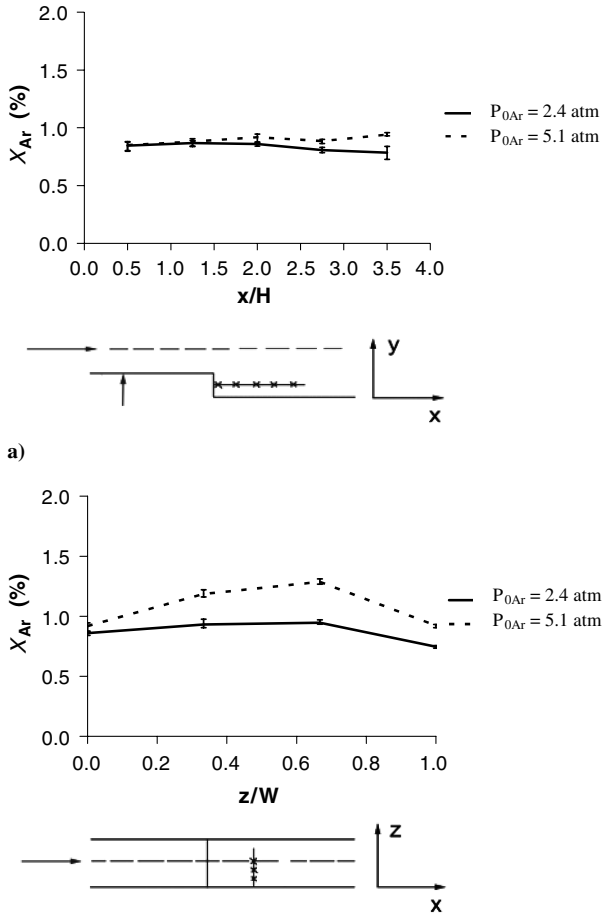

Fig. 11 Argon upstream injection; mole fraction distribution in the recirculation region for a) wall sampling and b) inflow sampling; $P_{0air} = 4.8$ atm and $M_{air} = 1.6$.

Table 4 Argon upstream fuel injection: global and local X_{Ar}

P_{0Ar}, atm	Local X_{Ar}, %	Global X_{Ar}, %	Local/global X_{Ar}
	Wall sampling		
2.4	0.7–0.9	0.2	3.3–4.0
5.1	0.8–1.0	0.5	1.7–2.0
	Inflow sampling		
2.4	0.7–1.0	0.2	3.3–4.5
5.1	0.9–1.3	0.5	1.9–2.8

If argon had been replaced by propane for $P_{0C_3H_8} = 2.4$ atm, the local $\varphi_{C_3H_8}$ would be estimated in the range of 0.2–0.3 for global $\varphi_{C_3H_8} = 0.06$; for $P_{0C_3H_8} = 5.1$ atm, the local $\varphi_{C_3H_8}$ would be estimated in the range of 0.2–0.3 for global $\varphi_{C_3H_8} = 0.1$. At the same flow rates, propane would have a 20% less dynamic pressure ratio and would cause even larger quantities of fuel to remain in the recirculation region.

Thus, for hydrocarbons, unlike the lighter hydrogen, the recirculation region is also expected to be fuel-rich with upstream injection, although considerably less than for direct base injection.

B. Reacting Flow

Chemically reacting cases involved air at $M_{air} = 1.6$, $T_{0air} = 300$ K, and $P_{0air} = 4.5$ atm and hydrogen at $P_{0H_2} = 4.5$ and 8.2 atm, resulting in dynamic pressure ratios of 0.5 and 1.0, respectively. It was injected from the base of the step and the upstream location.

1. Base Injection

The corresponding global φ_{H_2} was 0.04 and 0.08, respectively, for the conditions described earlier. The wall pressure distribution for the two P_{0H_2} is shown in Fig. 12. For $P_{0H_2} = 4.5$ atm, the expansion of airflow approaching the step is less pronounced than for the nonreacting case shown in Fig. 3, due to heat released from combustion resulting in the pressure rise at the step base. Hence, the recirculation region length is considerably larger than the corresponding nonreacting case and more air is available for mixing with the fuel. As the fuel flow is increased to $P_{0H_2} = 8.2$ atm, the local pressure increases even further and an even longer recirculation region is present. The shear layer does not reattach within the test-section length. Figures 13 and 14 show the local equivalence ratio φ_{H_2} and species concentration at the two pressures measured at the wall. The local φ_{H_2} were deduced from the mole fractions of hydrogen and water in the product mixture. The fuel-injection location is indicated on the horizontal axis in the plots. A highly nonuniform φ_{H_2} distribution is observed at the wall with a maximum around $2.2H$. The local φ_{H_2} reaches 0.7 at the lower pressure and up to $\varphi_{H_2} = 1.3$ at the higher pressure, showing a proportional increase due to an increase in fuel rate.

The combustion-products wall distribution for the two cases is shown in Figs. 13b and 14b. Consistent with the earlier observation

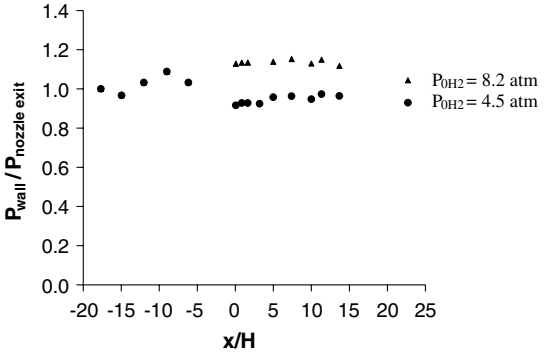

Fig. 12 Wall pressure distribution for hydrogen combustion; $P_{0air} = 4.8$ atm and $M_{air} = 1.6$; heat release increased the local pressure and enlarged the recirculation region.

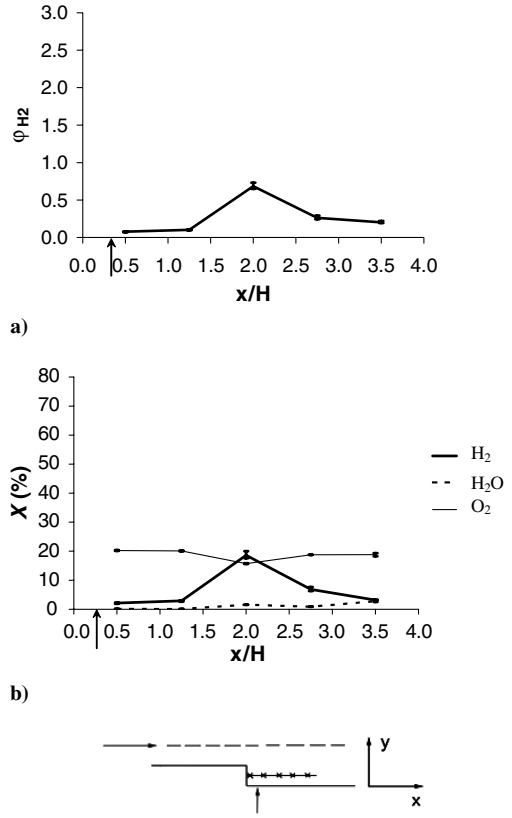

Fig. 13 Wall sampling results for hydrogen combustion: a) equivalence ratio distribution in the recirculation region and b) combustion species mole fraction distribution; $P_{0H_2} = 4.5$ atm.

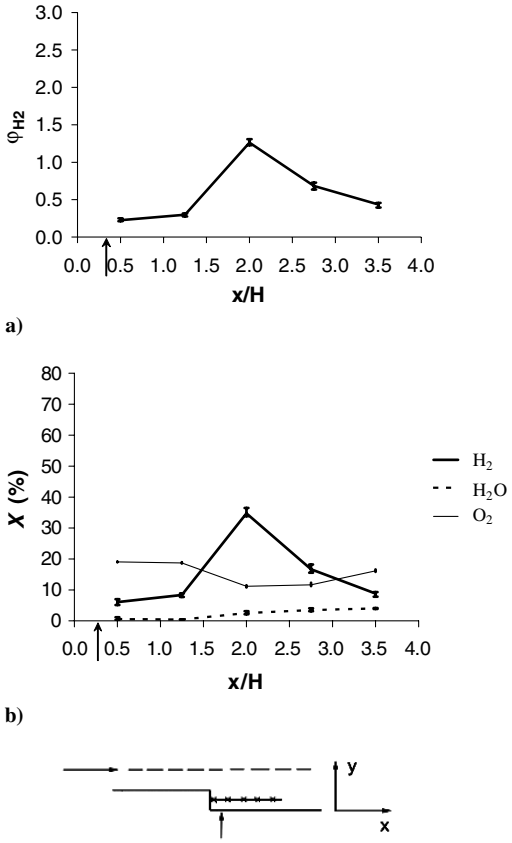

Fig. 14 Wall sampling results for hydrogen combustion: a) equivalence ratio distribution in the recirculation region and b) combustion species mole fraction distribution; $P_{0H_2} = 8.2$ atm.

of a fuel-rich mixture existing in the recirculation region, the combustion-product composition shows a significant proportion of unburned hydrogen. X_{H_2O} increases downstream of the step; however, a significant proportion of unburned oxygen and only a small proportion of water are noticed. This is a reflection of the conditions immediately in the vicinity of the cold wall on which the combustion radicals are quenched; hence, the composition can be quite different from elsewhere in the flow.

Therefore, more informative is the inflow sampling shown in Figs. 15 and 16. The inflow sampling locations are shown in the figures. The experimental conditions were not identical over the repeated tests: both P_{0air} and P_{0H_2} varied by 0.3 atm, resulting in the larger standard deviations observed in the plots due to changes in recirculation region composition. The local φ_{H_2} distributions in Figs. 15a and 16a show a decreasing amount of fuel downstream of the injection location. The local φ_{H_2} does not increase proportionally with the increase in P_{0H_2}. As the fuel rate increased, the local φ_{H_2} increased unevenly in the recirculation region; the region close to the injection location experienced a lower increase in φ_{H_2} than the region farther away in the x direction, in which more air was available for the chemical reactions. Thus, increasing P_{0H_2} led to a reduction of local gradients in the recirculation region. The product mole fraction distributions in Figs. 15b and 16b show a fuel-rich mixture in the recirculation region with considerable amounts of unburned hydrogen and almost no oxygen. The proportion of unburned hydrogen dropped rapidly downstream. For low fuel-flow rates, once the hydrogen was completely consumed, the oxygen mole fraction increased as air continued to enter the recirculation region. For high P_{0H_2}, hydrogen was still present at the last sampling port and oxygen was virtually nonexistent. The temperature drop of the sampled mixture while passing through the cooling jacket resulted in condensation of water vapor and much could not reach the mass spectrometer. Hence, the corrected X_{H_2O} was deduced from the oxygen deficit in the product mixture. Both corrected and uncorrected X_{H_2O} are plotted in the figures for comparison. Unlike the wall sampling experiments, a significant amount of water was

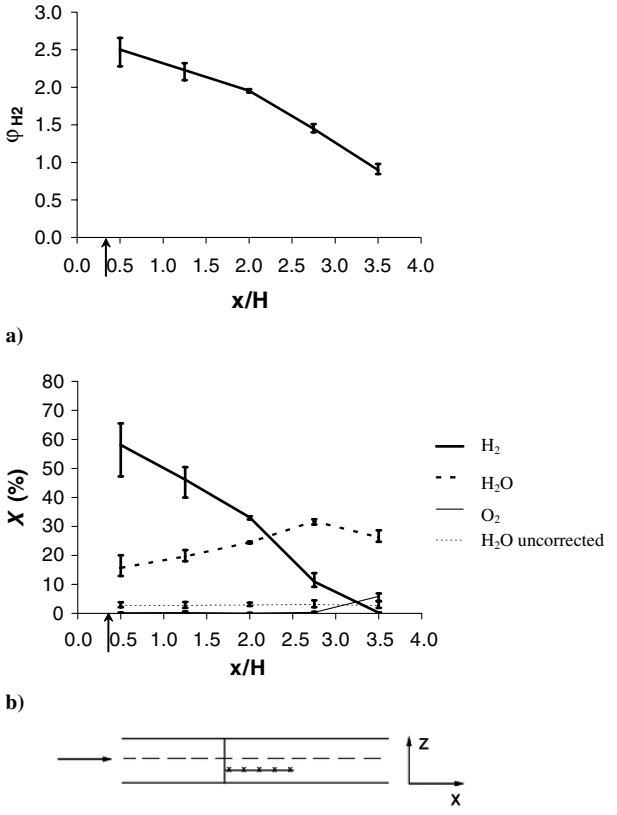

Fig. 15 Inflow sampling results for hydrogen combustion: a) equivalence ratio distribution in the recirculation region and b) combustion species mole fraction distribution; $P_{0H_2} = 4.5$ atm.

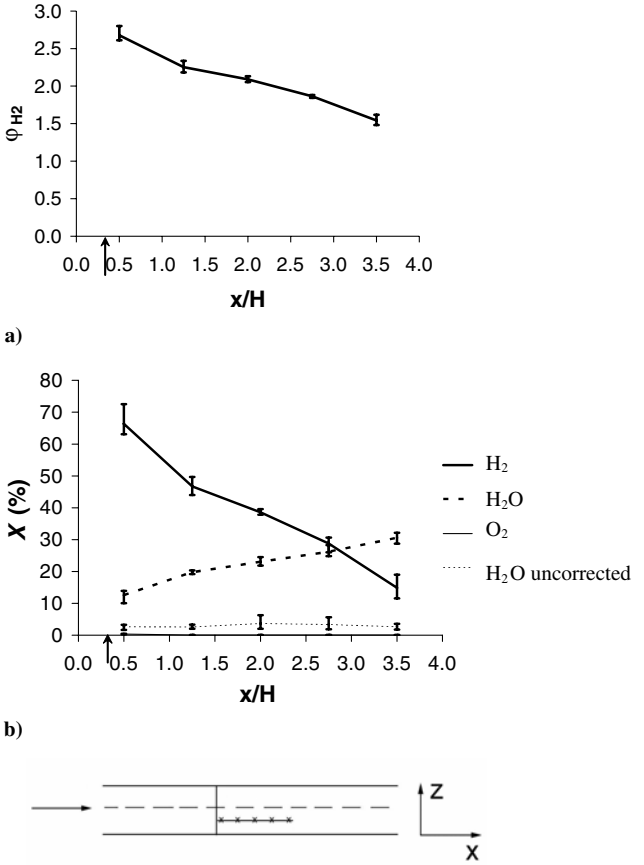

Fig. 16 Inflow sampling results for hydrogen combustion: a) equivalence ratio distribution in the recirculation region and b) combustion species mole fraction distribution; $P_{0H_2} = 8.2$ atm.

detected and X_{H_2O} increased downstream as mixing and combustion improved.

The local and global φ_{H_2} for the two P_{0H_2} obtained from wall and inflow samplings are compared in Table 5. Considerably more fuel is observed away from the wall. For both P_{0H_2}, the local φ_{H_2} was an order of magnitude higher than the suggested global value.

2. *Upstream Injection*

Hydrogen was injected upstream of the step for identical airflow conditions as base injection (i.e., $P_{0H_2} = 2.5$ and 8.2 atm). A stable flame could not be established at any of these conditions, which, given the results predicted by the nonreacting flow experiments with helium, indicate that insufficient fuel penetrated in the recirculation region to sustain a stable flame. A change in the injection configuration (e.g., number and/or size of orifices, angled injection, a different flameholder geometry, etc.) may lead to possibly holding the flame.

IV. Conclusions

Mass spectrometry (MS) and acetone PLIF were used to determine the species concentration distribution in the flameholding recirculation region formed behind a rectangular step in supersonic flow. Nonreacting and combustion experiments were conducted with

Table 5 Base fuel injection: global and local Φ_{H2}

P_{0H_2}, atm	Local Φ_{H_2}	Global Φ_{H_2}	Local/global Φ_{H_2}
		Wall sampling	
4.5	0.1–0.7	0.04	1.8–18.3
8.2	0.2–1.3	0.08	2.6–16.4
		Inflow sampling	
4.5	0.8–2.7	0.04	21.0–66.5
8.2	1.5–2.8	0.08	18.5–35.0

varied fuel-related parameters, including the injection location, injection pressure, and fuel type. The results showed the following:

1) The local fuel concentration in the recirculation region was found in some cases to be as much as an order of magnitude higher than suggested by the global fuel mole fraction because only small amounts of fresh air are entrained into the recirculation region.

2) This led to a predominantly fuel-rich recirculation region even when the global equivalence ratio was low, with noticeable differences depending on injectant molecular weight, injection location, and dynamic pressure ratio.

3) The local distribution varied considerably with large gradients closer to the step and considerably more uniform concentration distribution in the rest of the recirculation region.

4) The gradients extended further into the recirculation region as the fuel mass flow was increased. The fuel distribution pattern in the recirculation region was similar for both helium and argon. However, argon concentration in the recirculation region was higher than helium for a unit mole fraction of fuel injected in the test section. This is attributed to a slower diffusion rate of argon in air than that of helium.

5) Wall fuel concentration is considerable lower than in the rest of the recirculation region. This could be the result of fuel entrainment by wall-induced recirculations that normally form in a perpendicular direction to the main step recirculation.

6) Helium injected upstream tends to penetrate through the airflow boundary layer formed along the wall, and at both low and high dynamic pressure ratios, the fuel quantity detected in the recirculation region was comparable with or even less than the suggested global value.

7) The heavier gas, argon, remained in larger quantities in the boundary layer when injected upstream, and more fuel was detected in the recirculation region than indicated by the global value at both injection pressures.

8) With combustion, the increasing recirculation region size resulted in lower fuel distribution gradients compared with the nonreacting case.

9) The wall species distribution in the chemically reacting case is considerably different from the inflow measurement, due both to mixing and wall effects.

10) The recirculation region was rich at the base of the step, with the gradients rapidly dropping toward the downstream edge of the recirculation region.

Acknowledgment

This work was performed with support from NASA grant NCC3-994 with Claudia Meyer as the Program Manager.

References

[1] Ortwerth, P. J., Mathur, A. B., Segal, C. and Owens, M. G., "Combustion Stability Limits of Hydrogen in a Non-Premixed, Supersonic Flow," *14th International Symposium on Airbreathing Engines (ISABE99)* [CD-ROM], AIAA, Reston, VA, Sept. 1999.

[2] Dimotakis, P. E., "Turbulent Free Shear Layer Mixing And Combustion," *High-Speed Flight Propulsion Systems*, Progress in Aeronautics and Astronautics, Vol. 137, edited by S. N. B. Murthy and E. T. Curran, AIAA, Washington, DC, 1991, pp. 265–340.

[3] Ozawa, R. I., "Survey of Basic Data on Flame Stabilization and Propagation for High Speed Combustion Systems," U.S. Air Force Aero Propulsion Lab. Rept. AFAPL-TR-70-81, Wright–Patterson AFB, OH, 1971.

[4] Huellmantel, L. W., Ziemer, R. W., and Campbell, A. B., "Stabilization of Premixed propane–air Flames in Recessed Ducts," *Jet Propulsion*, Vol. 27, Jan. 1957, pp. 31–43.

[5] Baxter, M. R., and Lefebvre, A. H., "Weak Extinction Limits of Large-Scale Flameholders," *Journal of Engineering for Gas Turbines and Power*, Vol. 114, No. 4, 1992, pp. 776–782.

[6] Wright, R. H., and Zukoski, E. E., "Flame Spreading from Bluff Body Flameholders," Jet Propulsion Lab., California Inst. of Technology, Rept. 34-17, Pasadena, CA, 1960.

[7] Strokin, V., and Grachev, V., "Possible Scheme of Flameholding in Hydrogen Fueled Scramjet Combustors," *Proceedings of the First International Aerospace Congress*, Vol. 1, Moscow State Univ. of Aviation Technology, Moscow, 1994, pp. 630–633.

[8] Ogorodnikov, D. A., Vinogradov, V. A., Shikhman, Ju. M., and Strokin, V. N., "Design and Research Russian Program of Experimental Hydrogen Fueled Dual Mode Scramjet: Choice of Concept and Results of Pre-Flight Tests," AIAA Paper 98-1586, 1998.

[9] Driscoll, J. F., and Rasmussen, C. C., "Correlation and Analysis of Blowout Limits of Flames in High-Speed Airflows," *Journal of Propulsion and Power*, Vol. 21, No. 6, 2005, pp. 1035–1044.

[10] Rasmussen, C. C., Driscoll, J. F., Hsu, K. Y., Donbar, J. M., Gruber, M. R., and Carter, C. D., "Stability Limits of Cavity-Stabilized Flames in Supersonic Flow," *Proceedings of the Combustion Institute*, Vol. 30, Combustion Inst., Pittsburgh, PA, 2005, pp. 2825–2833.

[11] Winterfeld, G., "Stabilization of hydrogen–air Flames in Supersonic Flow," *Modern Research Topics in Aerospace Propulsion*, edited by G. Angelino, L. deLuca, and W. A. Sirignano, Springer–Verlag, New York, 1991, pp. 37–47.

[12] Hsu, K. Y., Carter, C. D., Crafton, J., Gruber, M. R., Donbar, J. M., Mathur, T., Schommer, D., and Terry, W., "Fuel Distribution About a Cavity Flameholder in Supersonic Flow," AIAA Paper 2000-3585, 2000.

[13] Gruber, M. R., Donbar, J. M., Carter, C. D., and Hsu, K. Y., "Mixing and Combustion Studies Using Cavity Based Flameholders in a Supersonic Flow," *Journal of Propulsion and Power*, Vol. 20, No. 5, 2004, pp. 769–778.

[14] Uchiumi, M., Kobayashi, H., Hasegawa, S., and Niioka, T., "Experiments on the Flameholding Mechanism of a Newly Devised Strut in Supersonic Airflow," *IUTAM Symposium on Combustion in Supersonic Flows*, Kluwer Academic, Dordrecht, The Netherlands, 1997, pp. 135–144.

[15] Niioka, T., Terada, K., Kobayashi, H., and Hasegawa, S., "Flame Stabilization Characteristics of Strut Divided into two Parts in Supersonic Flow," *Journal of Propulsion and Power*, Vol. 11, No. 1, 1995, pp. 112–116.

[16] Zamma, Y., Shiba, H., Masuya, G., Tomioka, S., Hiraiwa, T. and Mitani, T., "Similarity Parameters of Pre-Ignition Flowfields in a Supersonic Combustor," AIAA Paper 1997-2890, 1997.

[17] Thayer, W. J., and Corlett, R. C., "Gas Dynamic and Transport Phenomena in the Two-Dimensional Jet Interaction Flowfield," *AIAA Journal*, Vol. 10, No. 4, 1972, pp. 488–493.

[18] McDaniel, J. C., Fletcher, D., Hartfield, R., and Hollo, S., "Staged Transverse Injection into Mach 2 Flow Behind a Rearward-Facing Step: A 3-D Compressible Test Case for Hypersonic Combustor Code Validation," AIAA Paper 1991-5071, 1991.

[19] Morrison, C. Q., Campbell, R. L., Edelman, R. B., and Jaul, W. K., "Hydrocarbon Fueled Dual Mode Ramjet/Scramjet Concept Evaluation," International Society for Airbreathing Engines, Paper 1997-7053, 1997.

[20] Kim, C. K., Yu, S. T., and Zhang, Z. C., "Cavity Flow in Scramjet Engine by Space-Time Conservation and Solution Element Method," *AIAA Journal*, Vol. 42, No. 5, 2004, pp. 912–919.

[21] Glawe, D. D., Donbar, J. M., Nejad, A. S., Sekar, B., Chen, T. H., Samimy, M., and Driscoll, J. F., "Parallel Fuel Injection from the Base of an Extended Strut into Supersonic Flow," AIAA Paper 1994-0711, 1994.

[22] Owens, M. G., and Segal, C., "Development of a Hybrid-Fuzzy Air Temperature Controller for a Supersonic Combustion Test Facility," *Experiments in Fluids*, Vol. 31, No. 1, 2001, pp. 26–33. doi:10.1007/s003480000255

[23] Portz, R., and Segal, C., "Penetration of Gaseous Jets in Supersonic Flows," *AIAA Journal*, Vol. 44, No. 10, Oct. 2006, pp. 2426–2429. doi:10.2514/1.23541

[24] Lozano, A., Yip, B., and Hanson, R. K., "Acetone: A Tracer for Concentration Measurements in Gaseous Flows by Planar Laser-Induced Fluorescence," *Experiments in Fluids*, Vol. 13, No. 6, 1992, pp. 369–376. doi:10.1007/BF00223244

[25] Owens, M. G., Tehranian, S., Segal, C., and Vinogradov, V. A., "Flameholding Configurations for Kerosene Combustion in a Mach 1.8 Airflow," *Journal of Propulsion and Power*, Vol. 14, No. 4, July–Aug. 1998, pp. 456–461.

T. Lieuwen
Associate Editor